Composites Part B 214 (2021) 108735

Contents lists available at ScienceDirect

Composites Part B

journal homepage: www.elsevier.com/locate/composites

Modeling of anisotropic dual scale flow in RTM using the finite elements method

Silvio Facciotto [a,*], Pavel Simacek [b], Suresh G. Advani [b], Peter Middendorf [a]

[a] Institute of Aircraft Design, University of Stuttgart, Stuttgart, 70569, Germany
[b] Department of Mechanical Engineering and Center for Composite Materials, University of Delaware, Newark, DE 19711, USA

ARTICLE INFO

Keywords:
Liquid composite molding (LCM)
Resin transfer molding (RTM)
Dual scale flow modeling
Capillary action

ABSTRACT

In Liquid Composite Molding (LCM) processes, a fabric reinforcement is placed in a closed cavity and resin is injected into the mold. Almost all reinforcements are dual scale containing fiber tows, which fill at a different rate than the region in between the fiber tows. Simulation of LCM processes can help identify regions that fail to fill. However, the presence of dual scale flow is usually neglected. Here this phenomenon is modeled using Liquid Injection Molding Simulation (LIMS) software in which a complex network of one-dimensional elements is created. This allowed us to simulate transverse and longitudinal flow through the fiber tows taking into consideration the orientation and architecture of the reinforcement and, additionally, adding capillary effects to the model. A sensitivity study has been performed to investigate the effects of properties in non-dimensional form, allowing for comparison with experiments that were conducted to validate the model by visualization of the flow front position and dual scale area dimensions.

1. Introduction

Composite materials are known for their combination of high mechanical properties and lightweight, design flexibility and non-corrosive properties and hence have been making inroads in aerospace, automotive and trucking industries where fuel savings are very important. Among several production techniques, Liquid Composite Molding (LCM) is often used because it can make net shape components, is cost-efficient and can be adapted to manufacture medium to large volume of parts. Among the many techniques included in LCM, Resin Transfer Molding (RTM) is a common one in the modern industry as it allows the production of high quality composite parts with reasonable reproducibility. Such technique consists of injecting pressurized resin in a rigid mold containing dry fiber reinforcement. One of the biggest challenges associated with RTM are flow induced defects. Among these, the two most important are dry spots also known as macrovoids and meso or microvoids. The former are regions of preform devoid of resin and are easily recognizable by the naked eye. The latter occur at the meso and micro level and often require a more sophisticated evaluation tool to identify this defect. According to the American aeronautics standard [1], final products with more than 2% of voids should be rejected as this negatively influences the performance and safety of the structure. The presence of voids in the components deteriorates the mechanical properties of a part, reducing flexural and compressive strength [2,3] and interlaminar shear strength [4]. Therefore, predicting and preventing such defects will be a big advantage for the manufacturer to reduce potential material and economic waste. The biggest cause for microscale voids generation that can be identified in literature is the non-uniformity of the flow front [1,5–10]. The reinforcement materials used in the RTM process often are textiles with a complex architecture of tows, which interlace each other, defining two different regions that will be filled at different rates by the resin. This phenomenon is called dual scale flow and is related with the concept of microvoids and tow saturation.

1.1. Dual scale flow

As mentioned above, dual scale flow is generated in fibrous porous media that contain two different scales of pores. This is the case, for example, of textile preforms used in several composite manufacturing processes shown in Fig. 1(a), including RTM. For such fabric architectures the pores between the tows of the reinforcement will be filled first, leaving the smaller pores of the fiber tow unsaturated creating microvoids [11–13]. The creation of microvoids is due to dual scale flow. The permeability of the fiber tows, as shown by many authors in literature [14–17], is normally several orders of magnitude lower than the bulk preform. This creates a region in the preform, where

* Corresponding author.
E-mail address: facciotto@ifb.uni-stuttgart.de (S. Facciotto).

https://doi.org/10.1016/j.compositesb.2021.108735
Received 13 January 2021; Accepted 16 February 2021
Available online 19 February 2021

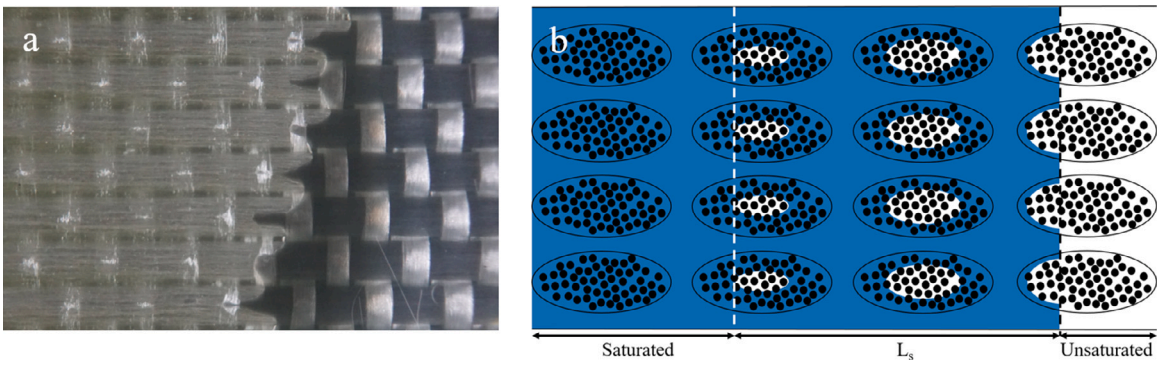

Fig. 1. Example of textile preform and dual scale flow impregnating first the spaces between and then the porous volume inside the fiber tows (a); Dual Scale Flow scheme showing saturated, partially saturated and unsaturated region (b).

the velocity of the flow front in the bulk and tow regions do not match. This leads to a partially saturated region, which can be defined with the saturation length Ls, where mechanical entrapment of voids can occur. The saturation length shown in Fig. 1(b) depends on the architecture of the reinforcement, the type of material used and the velocity of the flow front. Leclerc et al. and Ruiz et al. [5,9], showed that it is possible to find an optimal impregnation velocity, at which the total void content can be minimized. This can be expressed under the form of a modified capillary number and is deeply connected to the concept of saturation of the tows, as presented by Patel et al. [18–20]. The compacted tows lead to the presence of capillary pressure, which increases with the increase of compaction, and generates a higher pressure gradient in the tow regions, counteracting the low permeability of the tows. The same authors showed that depending on the velocity of the flow front, the flow inside the tows will be preferred over the one between them and vice versa, generating microvoids for fast flowing resin and macrovoids for slow filling. This is because at low velocities the capillary pressure due to the fiber tows becomes relevant and the flow between and inside the tows reach similar velocities. In some extreme cases the capillary pressure can influence the process so much that meso voids are created between the fiber tows [1,5,9,21,22] as shown in Fig. 2. Several authors explored the modeling of dual scale flow using several techniques and accounting for capillary pressure and the influence of the micro structure (tow scale) [23]. Pillai et al. numerically used a sink term in the equation of continuity of the macroscopic flows to solve for the dual scale flow [24]. Leclerc et al. and Ruiz et al. [5,9] modeled the generation of voids starting from experimental data and using a logarithmic model to predict and differentiate macro and microvoids. Lundström et al. [25] analyzed the impregnation of non-crimp fabrics and showed that perturbation in the bundle geometry affects the creation and dynamics of voids. Park et al. [1] modeled the generation and evolution of voids using a numerical approach accounting for compaction and movement and considering the micro structure of the tows. DeValve et al. developed a detailed numerical simulation of the impregnation of ideal plain weave architectures taking capillary effects into consideration and modeling the location, shape, size and evolution of air entrapment [26]. Gascón et al. presented a fractional flow model based on dual scale flow which is capable of simulating void formation and evolution [27]. Matsuzaki et al. showed that optimal flow velocity and void formation change with anisotropy of the reinforcement and developed a mathematical model for mesovoid formation [28]. Moreover they studied experimentally the effect of flow angle on final void content showing that this has an impact on the final outcome of the impregnation [29]. Liu et al. [30] modeled the formation of voids using a bifluid-solid contact model and implementing it in a finite elements framework. Arcila et al. [31] studied the phenomenon using the boundary element method, while Kang et al. [32] and Aaboud et al. [7] modeled the generation of voids comparing the times necessary to fill the macro and micro pores of the preform.

1.2. Simulation of dual scale flow with LIMS

Another approach was proposed by Simacek and Advani [8] using Liquid Injection Molding Simulations (LIMS). The software is a Finite Elements software developed at the University of Delaware, which, thanks to its scripting capabilities, allows the analysis of complex meshes with different types of elements which makes it possible to model dual scale flow by adding an external sink term instead of including it in the continuity equation. In fact, the simulation of dual scale flow can be performed by combining traditional governing equations such as Darcy's law:

$$\langle v\rangle = \frac{\overline{\boldsymbol{K}}}{\eta}\cdot\nabla P \tag{1}$$

and continuity equation (conservation of mass):

$$\nabla\cdot\langle v\rangle = 0 \tag{2}$$

where $\langle v\rangle$ is the volume averaged flow velocity, $\overline{\boldsymbol{K}}$ is the permeability of the porous medium which could be determined experimentally or found numerically [33], P the pressure, and η the viscosity of the injected resin. However, the loss of resin inside the fiber tows may be modeled by adding a sink term q to the continuity equation. The governing equation for dual scale flow assumes the form:

$$\nabla\cdot\left(\frac{\overline{\boldsymbol{K}}}{\eta}\cdot\nabla P\right) = q(P,s) \tag{3}$$

The sink term q is a function of the saturation s and pressure, P. Once the tow is completely filled, the saturation term disappears. The sink term can be introduced into the governing equations as presented by Park et al. [1], or externally by attaching one dimensional slave elements to the original 2D or 3D mesh that represents the part geometry as shown by Simacek and Advani and Kuentzer and Lawrence [8,13,34]. These slave elements attached to the nodes of the original mesh describe the resin flow inside the fiber tows. The effect of such elements, which share the nodes with the mesh representing the bulk preform, is drawing resin away from the mesh of the part which mimics what occurs during the dual scale flow. However, the additional porous volume must be accounted for to preserve the amount of porous volume of the original model, therefore the cross section of the tows, $A^{tow-adj}$ and the bulk volume fraction of the 2D or 3D elements of the original mesh, $V_f^{bulk-adj}$ have to be adjusted as shown:

$$A^{tow-adj} = V^{bulk}\left(\frac{V_f^{bulk}}{V_f^{tow}}\right)\left(\frac{2}{l}\right) \tag{4}$$

$$V_f^{bulk-adj} = V_f^{bulk}\left(1+2\left[\frac{1-V_f^{tow}}{V_f^{tow}}\right]\right) \tag{5}$$

Here V^{bulk} represents the original volume of the bulk element and l is the length of the one-dimensional slave elements, which is chosen

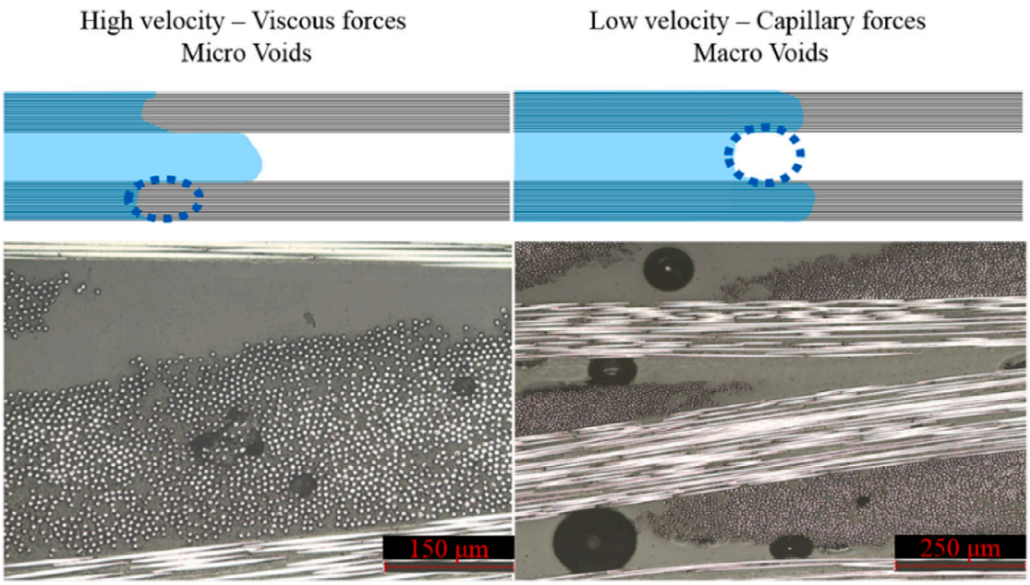

Fig. 2. Creation of microvoids inside the fiber tows and meso voids in between the fiber tows.

by measuring the dimensions of the tow, and V_f^{bulk} and V_f^{tow} are the volume fractions of the bulk and fiber tows respectively. Moreover, the cross section of the elements sharing nodes with the original mesh around the edges have to be changed accordingly to obtain equivalent control volumes [8]. Based on the modeling approach presented by the authors mentioned above, Gourichon et al. [35] and Schell et al. [36] showed that it is possible to model the generation and evolution of microvoids and mesovoids modifying the volume fraction content and fill factor to account for air entrapment in both elements representing the fiber tows and bulk preform. Finally, Lawrence et al. [34] showed that it is also possible to model the effect of capillary pressure by adding vents at the end of the slave elements. This required additional elements to control such vents and prevent the resin from leaving the mold.

2. Modeling dual scale flow with anisotropic tow permeability

The approach presented in [8,13,34] model saturation of the fiber tow by only considering the resin flow in the transverse direction relative to the fiber tow and without considering the architecture of the preform. However the saturation, and therefore possible air entrapment, is influenced by the anisotropy of the preform, especially in presence of local inhomogeneity, which might be created by complex shapes and textiles. Analytical models present in literature show that fabric micro structure, flow direction, and preform geometric anisotropy play a role in void formation [23]. The aim of this work is to implement a model capable of simulating the dual scale flow during the RTM process considering the anisotropic nature of the tow and the architecture of the fiber reinforcement without necessarily having to model complex micro structures. The modeling strategy used starts with meshing the geometry of the part. In this work a flat plate geometry has been analyzed using a regular mesh with 5 mm x 5 mm two-dimensional (shell) elements. The dimensions are 280 mm x 205 mm with a thickness of 2 mm and represent the cavity of the mold used for the experimental work to validate the model. The materials used for the simulation correspond to the materials used in the testing and validation part of this work. For the reinforcement, the quasi-UD glass plain woven fabric Interglas 92146 (425 g/m^2, with 550 tows per m (EC9-136x5t0) in warp direction and 630 tows per m (EC9-68) in weft direction) was chosen. The resin used was the epoxy resin system Hexion Epikote Resin MGS RIMR 235 with Hexion Epikote Curing-Agent MGS RIMH 237. In this work two different reinforcement layups have been analyzed, all the information regarding the process parameters are summarized in Table 1 along with the bulk properties and the reference ID that will be used in this paper to reference the cases studied. As mentioned previously, the use of one-dimensional elements allows the addition of a sink term externally and models the tows through an isotropic value of permeability. In order to be able to represent the anisotropic nature of the tows, a complex network of bar elements is created and attached to the geometry of the part. Such network consists of two families of one-dimensional elements, representing the transverse and longitudinal permeability of the tow. Moreover, in order to consider the architecture of the preform, the network is replicated on the bottom of the two dimensional structure. This allows simulating the flow in the warp and weft tows as shown in Fig. 3 by considering the properties corresponding to each family of tows (transverse and longitudinal permeability, and tow volume fraction) for both warp and weft tows. As in the original model, the addition of extra slave elements, and thus extra volume, has to be accounted to preserve the total amount of porous volume of the system. It is therefore necessary to adjust the cross section of the 1D elements considering the new elements added to the model. This is done adding the contribution of the family of bar elements representing the longitudinal permeability to Eq. (4). Since the model represents the flow inside of the tow with two elements, the fiber volume fraction between longitudinal and transverse elements is considered to remain constant. Moreover, the ratio τ of warp tows in the preform has been taken into account as the mass of resin will split between warp and weft elements. These changes are shown in Eqs. (6) and (7) below and implemented directly in the model.

$$A_{warp}^{tow-adj} = V^{bulk}\left(\frac{V_f^{bulk}}{V_{f-warp}^{tow}}\right)\left(\frac{2}{l_{t-warp}+l_{l-warp}}\right)(1-\tau) \tag{6}$$

$$A_{weft}^{tow-adj} = V^{bulk}\left(\frac{V_f^{bulk}}{V_{f-weft}^{tow}}\right)\left(\frac{2}{l_{t-weft}+l_{l-weft}}\right)(\tau) \tag{7}$$

where l_{t-warp} and l_{t-weft} are the lengths of the warp and weft tow elements respectively representing the transverse permeability of the tow and l_{l-warp} and l_{l-weft} are the lengths of the warp and weft elements representing the longitudinal permeability of the tow. The possible scaling of the mesh representing the bulk preform is accounted in the cross section adjustment, in which the volume of the bulk element is considered along with longitudinal and transverse one dimensional elements. The properties of the elements are summarized in Table 2.

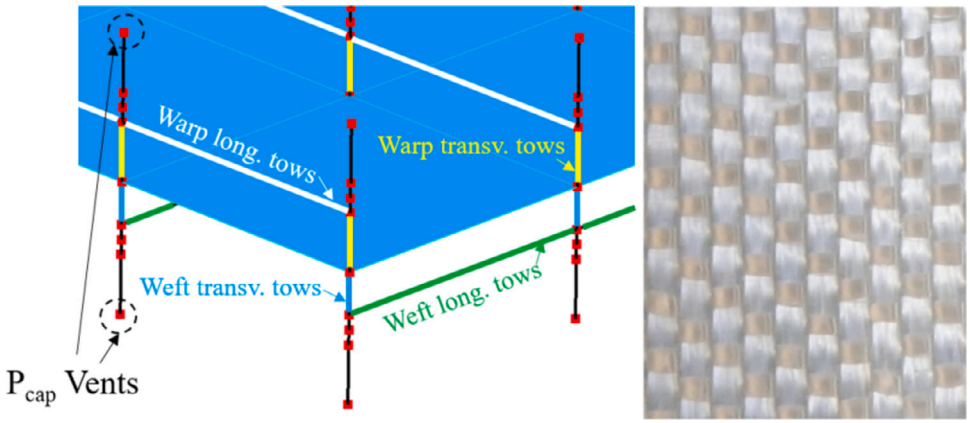

Fig. 3. Model of the fiber tows network to represent the dual scale flow which includes the capillary effect and picture of the woven glass fabric used in this work showing the architecture of the reinforcement. (For interpretation of the references to color in this figure legend, the reader is referred to the web version of this article.)

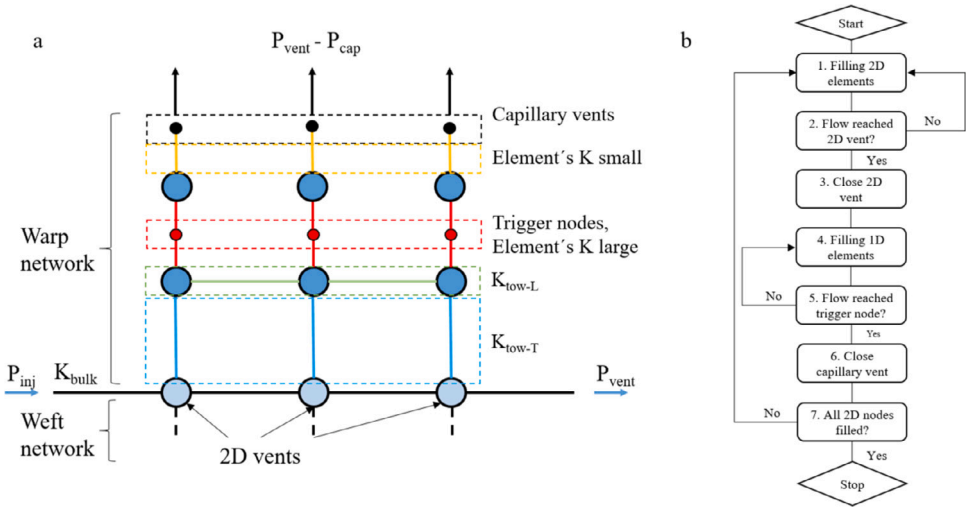

Fig. 4. Tows network scheme for modeling of capillary pressure (a). The first group of 1D elements (K_{tow-T}, blue in the picture) model the flow transverse to the fiber tows while the second group (K_{tow-L}, green) model the longitudinal flow. The red elements and nodes represent the trigger nodes system. The elements are assigned large permeability and small volume to avoid influencing the outcome of the model, their role is shown schematically in the flow chart beside (b). The last group of elements (yellow) consist of low permeability elements which prevent the resin from leaving the network through the vents placed at the end to model the capillary pressure. The same network is replicated along the bottom of the mesh to model the weft fibers. (For interpretation of the references to color in this figure legend, the reader is referred to the web version of this article.)

Table 1
Process parameters.

ID Plate	Layup	V_f^{bulk} [%]	$\triangle P$ [Pa]	η [Pa s]	K_{xx}^{bulk} [m^2]	K_{yy}^{bulk} [m^2]
A	$[0°]_6$	44	200000	0.26	1.76E−10	1.88E−11
B	$[90°]_6$	46	200000	0.26	1.88E−11	1.76E−10

The effect of capillary pressure was introduced using the modeling technique presented by Lawrence et al. [34]. A set of three bar elements were attached to each node in the tow network of one dimensional elements connected with the original mesh. These elements simulate the capillary pressure contribution by adding vents on the end node as shown in Fig. 3. The pressure of the system is set to satisfy Eq. (8):

$$P_{cap} = P_{vent} - P_{tow} \tag{8}$$

LIMS solves for the resin pressure and Eq. (8) can be satisfied by adding a pressure contribution to the model through the boundary condition of an inlet or a vent at a node. On the other hand, this means that the resin could potentially leave the system, which would be physically impossible. In order to prevent this, an element with very low permeability is placed between the vent and the node where the saturation of the tows is analyzed. Two additional elements are used to add a trigger node without impacting the total porous volume of the surrounding control volumes. This is done by assigning a very high permeability and very small length and cross section to such elements, ensuring that these elements do not affect the results of the simulation. The trigger node is used for closing the vent that models the effect of capillary pressure. Thus, the total pressure difference between the injection pressure and the vent of the mold is preserved by the model with the help of vents at each node of the shell elements of the original mesh of the part. Such additions are made by building the network for the slave elements, and by closing the vents right before the flow arrives there. The network of one-dimensional elements, shown in Fig. 4, is replicated for the weft tows as well, the only difference is the orientation of the longitudinal elements, which depends on the architecture of the reinforcement and is shown in Fig. 3.

2.1. Characterization of the tow parameters

The bulk properties of the preform and thus the permeability values that are assigned to the elements of the original mesh can be measured by standard permeability characterization techniques [37–41]. On the other hand, the properties of the fiber tows are more complex to characterize. The radius of single fibers composing the tows and the fiber

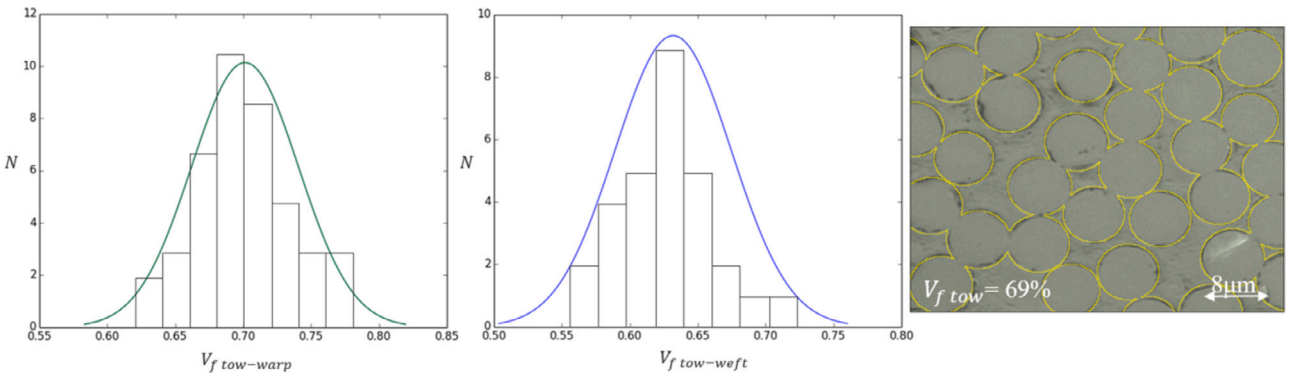

Fig. 5. Tow V_f measurements distribution for warp and weft tows and example of a measurement. N represents the number of measured tows that corresponded to the abscissa value.

Table 2
Tows properties as measured from the fabric used in experiments.

ID Plate	l_{t-warp} [mm]	l_{t-weft} [mm]	l_{l-warp} [mm]	l_{l-weft} [mm]	V_{f-warp}^{tow} [%]	V_{f-weft}^{tow} [%]	τ
A	0.5	0.358	5	5	69	63	0.583
B	1	0.715	5	5	69	63	0.583

Table 3
Parameters for permeability calculation.

Fiber arrangement	C_1	V_{fmax}	c
Quadratic	$\frac{16}{9\pi\sqrt{2}}$	$\frac{\pi}{4}$	57
Hexagonal	$\frac{16}{9\pi\sqrt{6}}$	$\frac{\pi}{2\sqrt{3}}$	53

volume fraction of the tows was measured using a microscope both for the warp and weft tow and the distribution of the measured volume fractions is shown in Fig. 5. Once the values of V_f^{tow} were measured, they were used to calculate theoretical values of tow permeability with the analytical model presented by Gebart [14]:

$$K_l = \frac{8R^2}{c}\frac{(1-V_f)^3}{V_f^2} \tag{9}$$

$$K_t = C_1\left(\sqrt{\frac{V_{fmax}}{V_f}}-1\right)^{\frac{5}{2}} R^2 \tag{10}$$

Where R is the radius of the fibers, V_{fmax} is the maximum volume fraction achievable and C_1 and c are constants depending on the distribution of the fibers inside the fiber tow. The values of these parameters are summarized in Table 3 [14]. The values of permeability obtained using the model represent a starting point for the analysis of the model and its validation. Both quadratic and hexagonal arrangement configurations have been implemented and used in the model, leading to less permeable tows for the quadratic configuration compared to the hexagonal if the fiber volume fraction is kept constant. The implementation of both arrangements allowed to determine a range of possible predictions of flow front positions and saturation lengths.

2.2. Capillary pressure analysis

Several authors in literature studied the characterization of capillary pressure and capillary effects. LeBel et al. [42] obtained the capillary properties and optimal impregnation velocity in the form of optimal capillary number (Ca^*) analyzing capillary flow using a fluorescence method. Pucci et al. [43] used wicking experiments and tensiometric technique to obtain capillary pressure analyzing textile preforms in different orientations. A simple capillary rise experiment allowed the determination of a range of possible capillary pressure values to be used in the simulation model. The test depicted in Fig. 6(a) consisted of immersing two glass capillary tubes of different diameters in a resin bath prepared with the resin used for the validation experiments. By measuring the height of the resin inside the capillary tubes it was possible to determine an approximate value for the surface tension using Eq. (11):

$$\gamma = \frac{\rho r g h}{2\cos\theta_{rc}} \tag{11}$$

Where ρ is the density of the resin, θ_{rc} is the contact angle formed by the meniscus of resin in the capillary tube, r the radius of the tube, and h the height reached by the resin inside the capillary. Positioning a micro droplet of resin under the microscope allowed the measurement of the static contact angle θ_{rf} between fiber and resin as shown in Fig. 6(b). This value, along with the diameter D_f of a fiber inside the tow, which was obtained by analyzing section cuts of cured specimens under the microscope, and the approximate value of surface tension obtained with the capillary rise method was used in Eq. (12) [44] to calculate a range of capillary pressure values which were used in the simulation and are listed in Table 4:

$$P_{cap} = \frac{F}{D_f}\frac{V_f^{tow}}{1-V_f^{tow}}\gamma\cos\theta_{rf} \tag{12}$$

Where F is the shape factor (2 for flow in the transverse direction and 4 for axial flow). For better accuracy, the dynamic advancing contact angle between fibers and resin should be considered [43]. However for this work a first approximation of the capillary pressure was considered sufficient and a wide range of values was examined in Section 4.1 to determine the sensitivity of the model to this parameter.

3. Validation of the model

The process of validating the model described in this work consisted of two steps. The first one consisted of comparing the flow front position during the experiments with the values predicted with the simulations. The second one was the analysis of the partially saturated area, where the dual scale flow was prevalent. The geometry chosen for the experimental analysis is a 280 mm x 205 mm x 2 mm rectangular, flat panel. This corresponds to the cases simulated and described in the previous sections. The mold used consisted of an aluminum bottom and an acrylic glass top to visualize the flow and saturation flow front. The top was reinforced with an aluminum cross-shaped frame to increase the stability and minimize deformation. The schematic of the setup is shown in Fig. 7. The analysis of the experimental process

Table 4
Capillary pressure parameters and range at 20 °C.

Contact angle θ_{rf} [°]	Surface tension γ [N/m]	Fiber Diameter [mm]	P_{cap} [Pa] – Range $F = 2$	P_{cap} [Pa] – Range $F = 4$
20–22	0.047	0.0082–0.0105	14133–18724	36195-47953

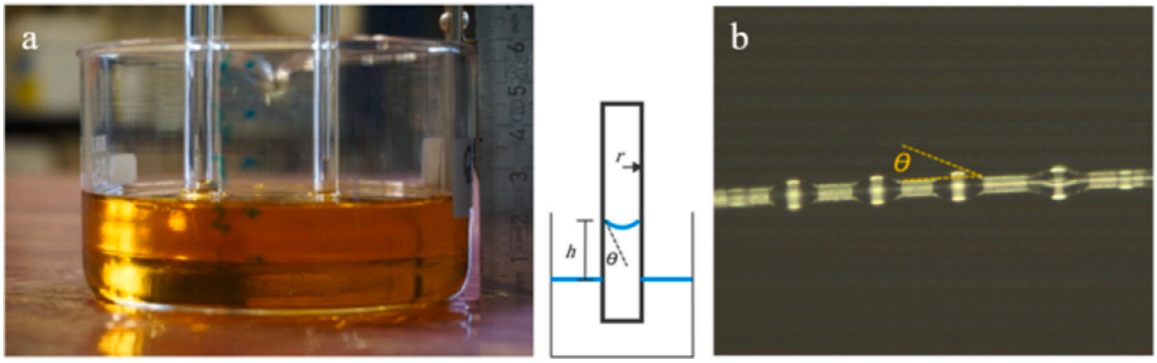

Fig. 6. Capillary rise test (a) and contact angle measurement (b).

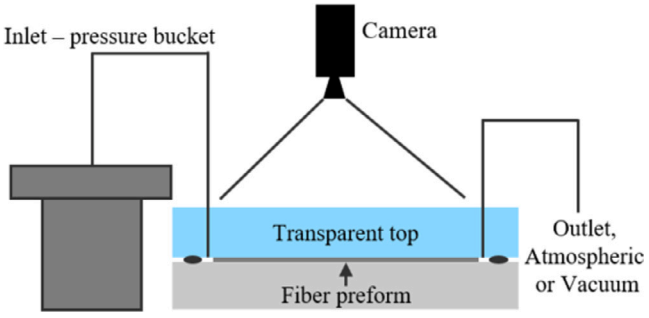

Fig. 7. Schematic of the experimental setup with a transparent top to visualize the flow and saturation front.

was performed optically using a camera positioned on top of the mold and a second camera provided with a macro-lens for the analysis of the dual scale flow where necessary. Two fiber preform layups were explored. In the first one (Plate A) the fiber preform was aligned in the direction of flow and in the second one (Plate B) the fiber preform was orthogonal to the direction of flow.

3.1. Flow front validation

Flow front tracking in the simulation for both layups used bulk permeability values obtained with the radial test rig present at the institute of aircraft design of the University of Stuttgart used in the benchmark exercise presented by May et al. regarding radial in plane permeability characterization [41] and are listed in Table 1. In order to compare and validate the simulation results, only experiments with no presence of race-tracking were taken into consideration. To avoid the occurrence of such phenomenon the edges of the mold were sealed using a thin layer of tacky tape, which successfully resulted in uniform resin flow across the width of the mold. The experiments conducted were repeated 3 times for each configuration and compared with the simulation model using both quadratic and hexagonal fiber arrangements. As visible in Fig. 8 the range of possible flow fronts generated by the simulation is in good agreement with the experimental results for plate B. For what concerns Plate A, the value of permeability obtained using Gebart's model [14] resulted in faster filling and wider dual scale flow compared to the tests. In order to reproduce the experimental results the value of tow permeability was increased and a comparable result was found for permeability values bigger of one order of magnitude, these results, labeled as "Calibrated", are also visible in Fig. 8. Increasing the permeability of the tows in the elements has a twofold effect on the model: increasing the saturated area and increasing the time necessary to completely fill the reinforcement, which also is in agreement with the results presented by Lawrence et al. [34].

3.2. Saturation length validation

The second validation performed was the analysis of the saturation length. The saturation length L_{sat} is defined as the distance between the flow front and the fully saturated flow. This parameter, shown in Fig. 1(b) and Fig. 9, can be translated into $\frac{x_{sat}}{L}$, representing the percentage of completely saturated reinforcement (x_{sat}) over the length of the mold, L. This allows one, in combination with the flow front prediction, to determine whether the permeability selected for the fiber tows is appropriate and represents the dual scale flow properly. The measurement of such length was performed optically for all the experiments as shown in Fig. 9 and compared with the results of the simulation model. Due to the necessity of sometimes magnifying the dual scale zone in order to determine the saturation length, it has been necessary to measure L_{sat} first and then convert it to the parameter $\frac{x_{sat}}{L}$ by relating the percentage of saturated fibers with respect to the flow front position x_{ff} as shown in Eq. (13):

$$\frac{x_{sat}}{L} = \frac{x_{ff} - L_{sat}}{L} \tag{13}$$

The parameter x_{sat} was evaluated by measuring the distance between the inlet and the last fully saturated node, which is visible in Fig. 10. As for the validation of the flow front, the model representing case B (corresponding to the fibers positioned perpendicular to the flow front) was in good agreement with the results of the experiments. The values of tow permeability obtained using Gebart's model [14] resulted in the correct representation of the evolution of the dual scale flow as visible in Fig. 10(b). On the other hand, the model representing case A, analogously to the flow front validation of Section 4.1, presented different dual scale flow prediction, resulting in a wider saturation length compared with reality, which implies that a low value of permeability was chosen to represent the impregnation of the tows. In order for the model to represent properly the saturation of the plate the permeability of the tows was increased of one order of magnitude and results, labeled as "Calibrated", are visible in Fig. 10.

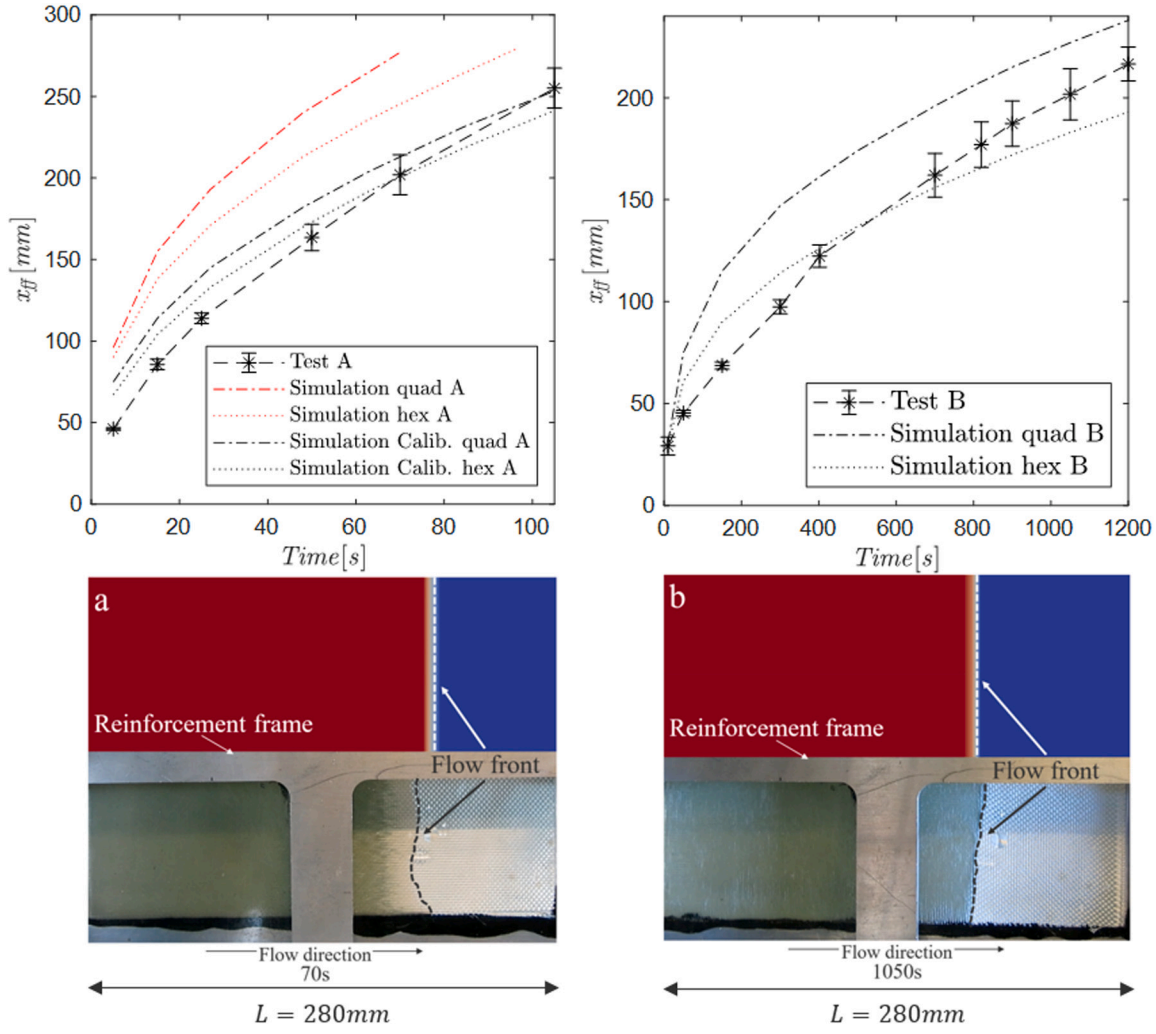

Fig. 8. Validation of flow front position: (a) Plate A (0° layup) test results with simulation predictions with tow permeability calculated with Gebart's model (red lines) and increasing the value of tow permeability of one order of magnitude (black line), (b) Plate B (90° layup) test results with tow permeability calculated with Gebart's model. Lower figure shows a snapshot of flow front position in the experiment and the simulation. Experimental flow front was averaged in the flow direction for comparison. (For interpretation of the references to color in this figure legend, the reader is referred to the web version of this article.)

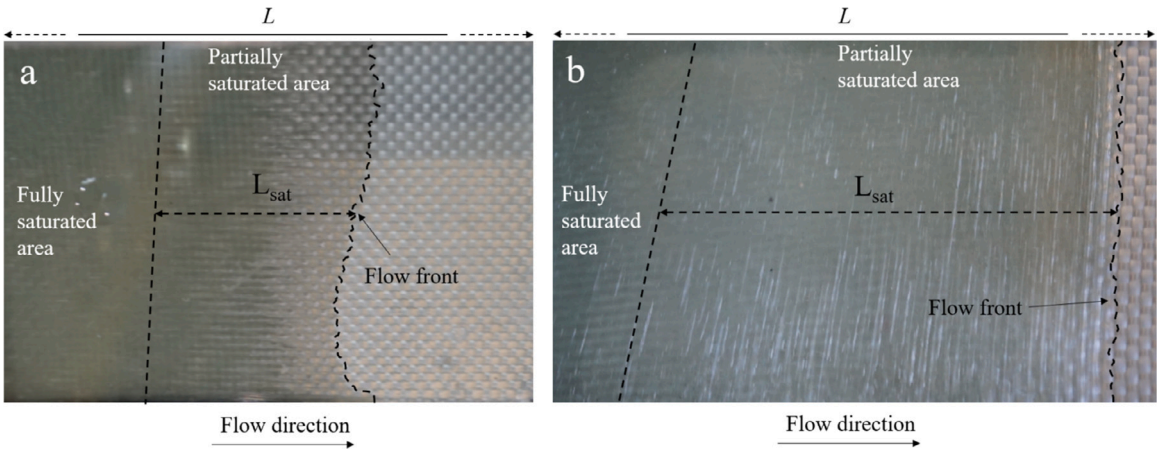

Fig. 9. Saturation length (L_{sat}) measurement: (a) Plate A (0° Layup); (b) Plate B (90° Layup).

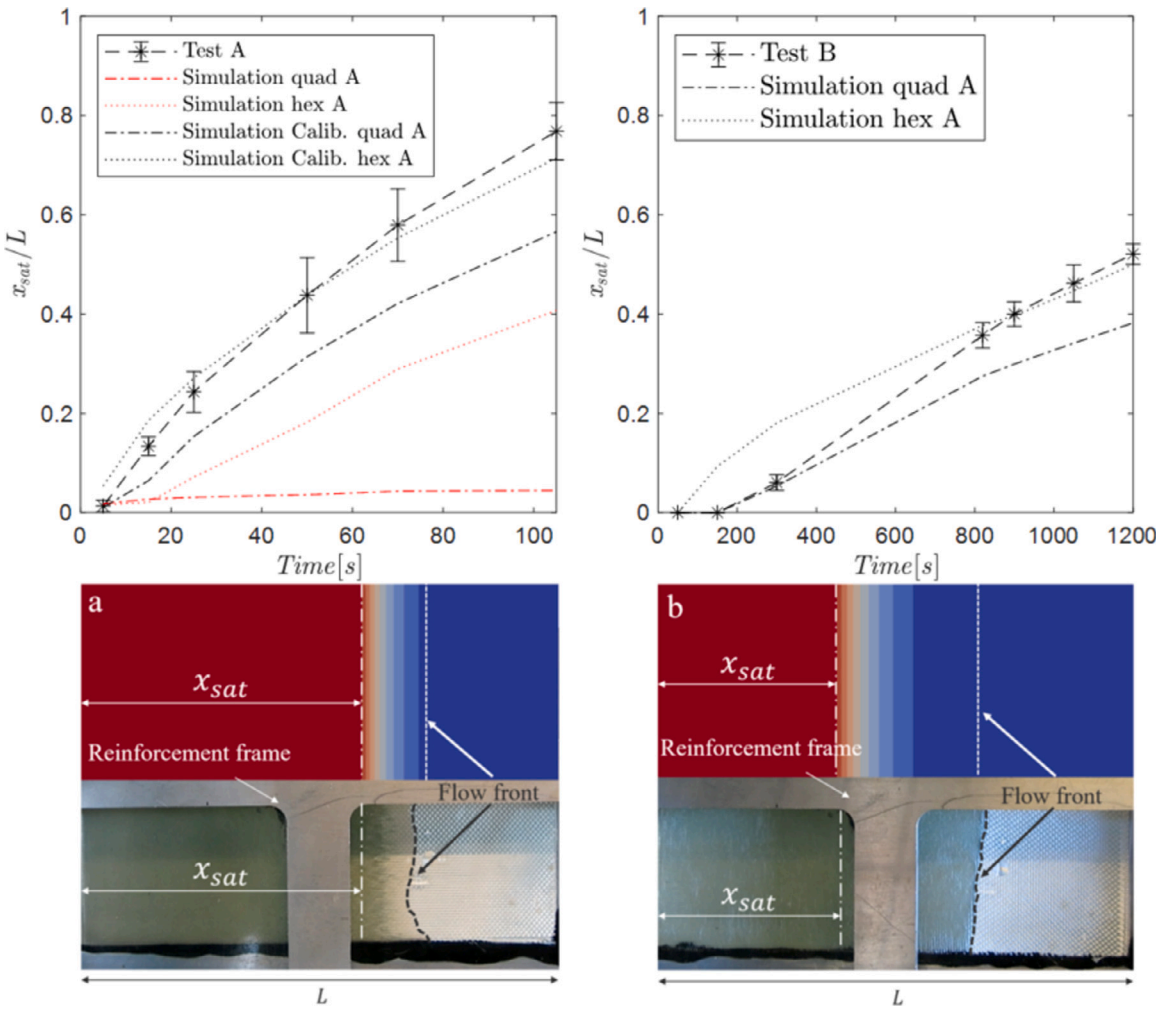

Fig. 10. Dual scale flow validation: (a) Plate A: comparison of dual scale flow between test and simulation with Gebart's model values (red lines) and simulation with modified tow permeability (black lines); (b) Plate B: comparison of dual scale flow between test and simulation with Gebart's model values. (For interpretation of the references to color in this figure legend, the reader is referred to the web version of this article.)

4. Parametric study

To explore the sensitivity of the model to the material and process parameters a numerical study was performed. Specifically two parameters influencing the degree of saturation were analyzed, namely the properties of the fiber tows and the effects of the capillary pressure. Both parameters are independent and impact the final saturation level, therefore can be included independently or together in the model. The degree of saturation of the filled part was analyzed in the same way as presented by Lawrence et al. [34] in which the ratio of completely saturated tow length, x_{sat}, over the length of the mold, L is expressed this time as a function of three independent variables as follows:

$$\frac{x_{sat}}{L} = f(C, \alpha_t, \alpha_l) \tag{14}$$

Here C, defined in Section 4.1, represents the capillary ratio, while α_t and α_l, defined in Sections 4.2 and 4.3, represent the effect of time scale on filling the mold over transverse and longitudinal tows respectively.

4.1. Effect of capillary pressure on saturation

The effect of capillary pressure was studied in the same way presented by Lawrence et al. [34] by defining the capillary ratio parameter as follows:

$$C = \frac{P_{cap}}{P_{inj}} \tag{15}$$

Where P_{cap} is the capillary pressure applied in the model and P_{inj} is the constant pressure applied at the inlet of the mold. The study is conducted for both A and B layups in which the flow is parallel and perpendicular to the fiber directions respectively. For these cases saturation shows different behaviors depending on the speed of the flow front and the properties of the tows. The results for the study are presented in Fig. 11, where the value of $C = 0$ corresponds to the case where no capillary pressure effects are modeled. This study shows that when the difference between the injection pressure and capillary pressure decreases, the saturation of the plate increases. Moreover, it is also possible to notice that for the case B, corresponding to the fibers placed at 90°, the effect of capillary forces is noticeable especially for the warp fibers, where the level of saturation is lower compared to the weft tows. The same is true for the case A with the tow permeability calculated with Gebart's model, corresponding to fibers placed at 0°. On the other hand, for the case of increased permeability which was presented in the validation section of this paper, the dual scale flow is drastically reduced and, due to the fast flow front, the effect of capillary pressure become less relevant for the final saturation value.

4.2. Effect of transverse tows

The dual scale flow is strongly dependent on the properties of the fiber tows, such as permeability and volume fraction. The time required to fill and saturate the additional bar elements plays an important

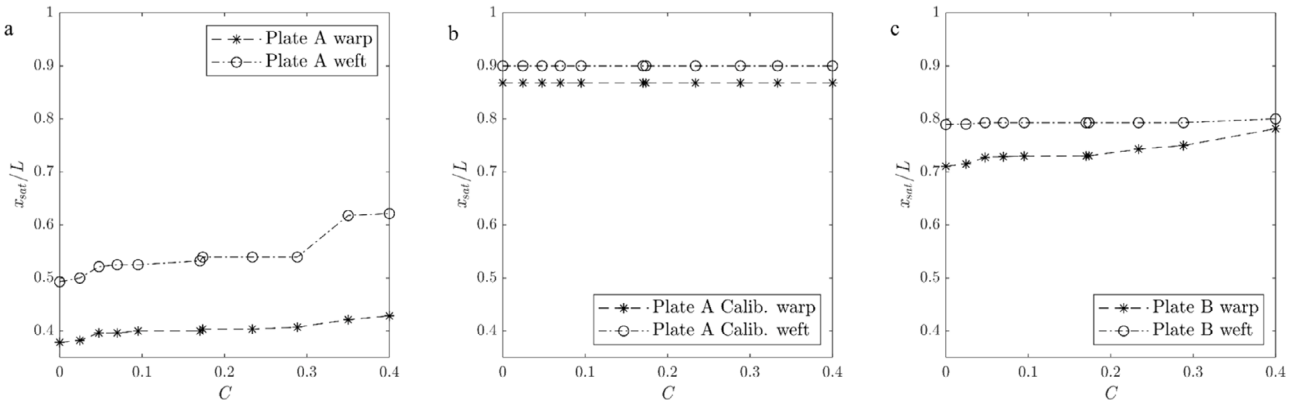

Fig. 11. Saturation dependence on capillarity for (a) Plate A (0° Layup), (b) Plate A with values of tow permeability increased by one order of magnitude as presented in Section 4 (0° Layup), and (c) Plate B (90° Layup).

role in terms of saturation. In reality the same effect is visible, where microvoids are created because of the difference in time required to fill the gaps between the tows as compared to between the fibers. In order to analyze the effect of such time scale difference, the parameter α_t is used. This was modified from the one used by Lawrence et al. [34] by adding the porosity content of the bulk preform $(1 - V_f^{bulk})$ and fiber tow $(1 - V_f^{tow-t})$ as follows:

$$\alpha_t = \frac{L_{mold}^2 K_{tow-t}(1 - V_f^{bulk})}{L_{tow-t}^2 K_{bulk}(1 - V_f^{tow-t})} \tag{16}$$

Where L_{mold} represents the length of the mold cavity, L_{tow} is the length assigned to the bar elements, K_{tow-t} is the permeability of the elements representing the flow in the transverse direction, which corresponds to the radius of the fiber tows, and K_{bulk} is the permeability of the bulk preform. Such parameter allows one to study the time required to fill the mold with respect of filling a fiber tow close to the inlet. In order to keep the relationship between warp and weft tows consistent in this sensitivity study, the analysis of α_t was performed scaling equally the values of warp and weft tow permeability. Compared to the values presented by Lawrence et al. in their study [34] the ratio α_t has noticeably higher values due to the difference in tow and bulk permeability for the materials used. In fact for the material used in this work the permeability of the tows calculated with Gebart's model is 3 orders of magnitude higher than the one presented by the Lawrence et al. in their paper. The results of the analysis are depicted in Fig. 12 for all the cases studied in this paper. It is visible how the parameter influences the saturation of the tows, by increasing the time needed to fill the mold over the time to fill one tow, the saturation increases for both warp and weft tows.

4.3. Effect of longitudinal tows

In a similar way, the effect of longitudinal tows was analyzed. Eq. (17) was modified to calculate the time to fill a longitudinal tow near the inlet.

$$\alpha_l = \frac{L_{mold}^2 K_{tow-l}(1 - V_f^{bulk})}{L_{tow-l}^2 K_{bulk}(1 - V_f^{tow-l})} \tag{17}$$

As for the previous case of Section 4.2, also for the analysis of α_l both values of tow permeability for warp and weft were scaled equally, maintaining the ratio of warp to weft fibers consistent within the analysis. The results obtained for the two cases studied can be seen in Fig. 13. It is noticeable that the sensitivity of the model related to the longitudinal tows decreases with decreasing difference between the tow and bulk filling and also that the model is more sensitive to changes in the transverse tow permeability values than longitudinal values. However, the flow inside the fiber tows in the axial direction still contributes to the saturation of the preform and the final quality of the part, becoming important when local effects are present in the impregnation process. This is shown in Section 5. Another important observation is regarding the orientation of the longitudinal elements, which corresponds to the orientation of the warp and weft fibers. In the case of fibers directed in the flow front direction, the effect of the longitudinal elements is noticeable, on the other hand the fibers orthogonal to the flow do not contribute to the saturation significantly. This means that in a more complex geometry with non-unidirectional flow the orientation of the longitudinal tows for both warp and weft fibers would contribute to the final outcome of the model and saturation. This was experimentally demonstrated by Matsuzaki et al. [29] and potentially allows the analysis of more complex reinforcement architectures.

5. Variability study

The fiber tows analyzed for the parameter characterization showed high variability in terms of fiber volumes fraction. This is due to several factors, the orientation of the preform, the nesting level, local imperfections of the reinforcement which leads to extra compaction etc. This might generate local inhomogeneity in the final saturation of the part. In order to study this, the normal distributions obtained from the tests and shown in Fig. 5 has been implemented in the model. For each fiber tow element, including both longitudinal and transverse bar elements, a random value based on the normal distribution of the tow fiber volume fraction is generated and a permeability is calculated using Gebart's model [14]. The same cases studied in the previous sections were studied applying this variability and resulted in complex patterns of saturation, which showed some similarities with the experiments performed. In particular, one interesting outcome of this model was shown by analyzing case B, where voids were trapped behind the flow front locally as shown in Fig. 14. Moreover the addition of one dimensional elements in the axial direction contributed in the saturation of some of the voids left behind, showing the benefit of the model compared to the original one. This analysis is only a first step of a possible variability study which can be performed using the model presented in this paper and requires further work.

6. Summary and conclusions

In the following work a simulation model has been presented, which is capable of taking into account the anisotropic nature of fiber tows without having to generate a micro structure and analyze the dual scale flow on the micro level. The method presented in this work reproduces dual scale flow without having to increase the computational time excessively. The model consists of one dimensional elements which are attached to the mesh of the part and organized in a

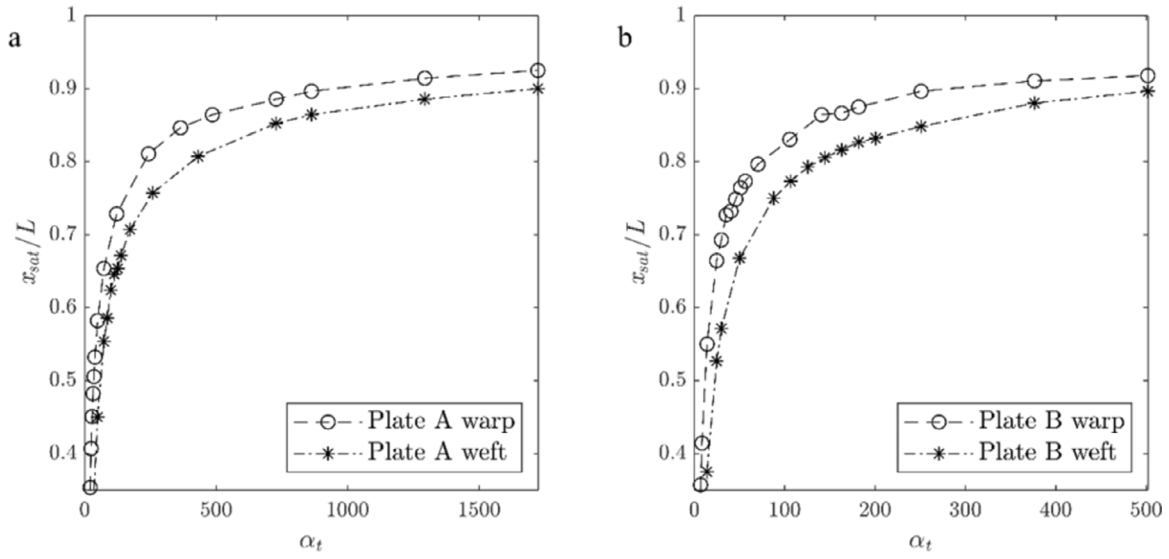

Fig. 12. Saturation dependence on transverse tow properties. Increasing the parameter α_t increases the ease of saturating the fiber tows, which reflects an increase of the time required to fill the mold. The values of α_t for Plate A (a) results considerably higher due to the higher bulk permeability for this layup configuration (0° Layup) compared to (b) Plate B (90° Layup).

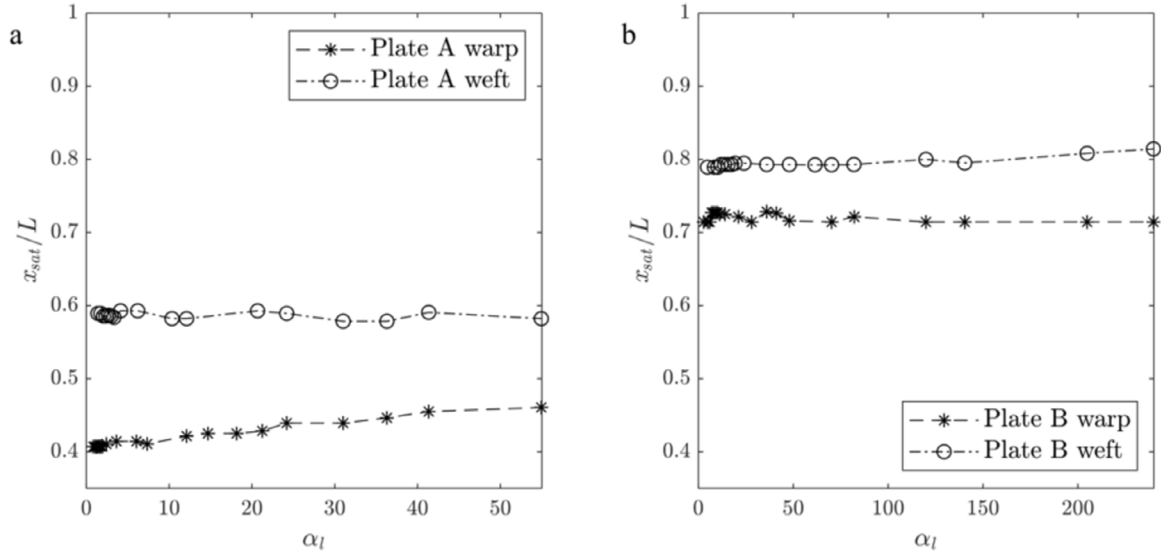

Fig. 13. Saturation dependence on longitudinal tow properties.

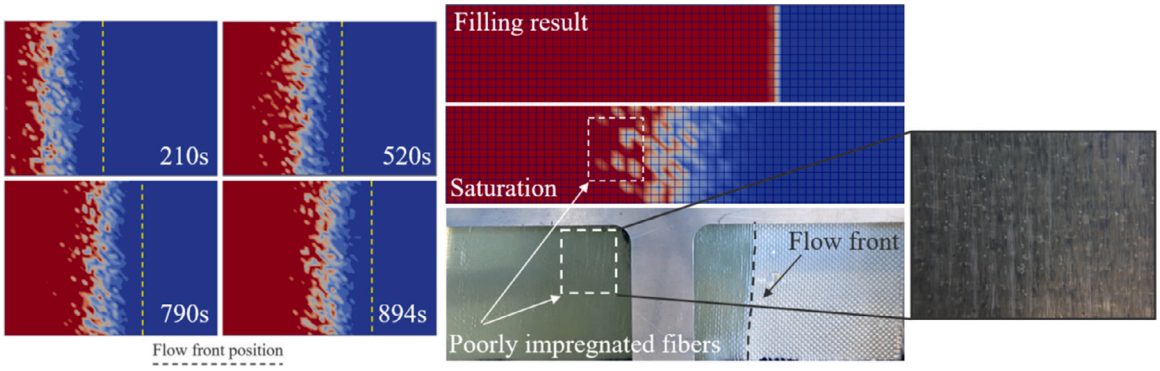

Fig. 14. Saturation pattern at infusion times 210 s, 520 s, 790 s and 894 s based on variability of Tow V_f and comparison with experiment. Although the value of x_{sat} remains on average the same as for the model with constant tow permeability, it is visible how some voids are left behind and are not impregnated completely. This is comparable to the experiments performed in this work.

complex network. Such network represents the flow of resin transverse and longitudinal to the fiber tow and, moreover, allows the addition of capillary pressure to the model. The variation of orientation and properties of the slave elements makes it possible to model complex reinforcements. Potentially the model could be extended to represent multiple layers of the reinforcement with additional layers of bulk mesh connected through the one dimensional elements. However this would increase the computation time and requires further investigation. The parameters used to model the dual scale flow have all been obtained from experiments apart from the permeability values of the tows, which were calculated using Gebart's analytical model [14] and successively calibrated through a numerical study. The sensitivity study allowed one to understand the effects of material properties and capillary pressure on the final saturation of the part. It was observed that decreasing the time scale for infusing the fiber tows and the bulk preform increases the quality of saturation. This means that to improve the quality of the part the use of slow filling can be beneficial. Finally, a variability study showed how the variability of the fiber volume fraction at the micro level can locally influence the saturation of the part leading to localized air entrapment.

CRediT authorship contribution statement

Silvio Facciotto: Conceptualization, Investigation, Methodology, Software, Validation, Visualization, Writing - original draft, Writing - review & editing. **Pavel Simacek:** Conceptualization, Methodology, Software, Supervision, Writing - review & editing, Resources. **Suresh G. Advani:** Conceptualization, Supervision, Writing - review & editing, Resources, Funding Acquisition. **Peter Middendorf:** Supervision, Writing - review & editing, Resources, Funding Acquisition.

Declaration of competing interest

The authors declare that they have no known competing financial interests or personal relationships that could have appeared to influence the work reported in this paper.

Acknowledgments

The present work is funded by the Deutsche Forschungsgemeinschaf (DFG, German Research Foundation) - Project number: 432847151 and partially funded by National Science Foundation (USA). NSF Organization: CMMI Div Of Civil, Mechanical, & Manufacturing Innovation Award No.: 2023323 which are gratefully acknowledged by the authors.

References

[1] Park CH, Woo L. Modeling void formation and unsaturated flow in liquid composite molding processes: a survey and review. J Reinf Plast Compos 2011;30(11):957–77. http://dx.doi.org/10.1177/0731684411411338.

[2] Greszczuk LB. Compressive strength and failure modes of unidirectional composites. In: Whitney JM, editor. Analysis of the Test Methods for High Modulus Fibers and Composites. ASTM STP 521, Philadelphia, Pa: American Society for Testing and Materials; 1973, p. 192–192–26. http://dx.doi.org/10.1520/STP36486S.

[3] de Almeida, Sérgio Frascino Müller, Neto, Zabulon dos Santos Nogueira. Effect of void content on the strength of composite laminates. Compos Struct 1994;28(2):139–48. http://dx.doi.org/10.1016/0263-8223(94)90044-2.

[4] Bowles KJ, Frimpong S. Void effects on the interlaminar shear strength of unidirectional graphite-fiber-reinforced composites. J Compos Mater 1992;26(10):1487–509. http://dx.doi.org/10.1177/002199839202601006.

[5] Leclerc JS, Ruiz E. Porosity reduction using optimized flow velocity in resin transfer molding. Composites A 2008;39(12):1859–68. http://dx.doi.org/10.1016/j.compositesa.2008.09.008.

[6] Aaboud B, Saouab A, Nawab Y. Simulation of air bubble's creation, compression, and transport phenomena in resin transfer moulding. J Compos Mater 2017;51(29):4115–27. http://dx.doi.org/10.1177/0021998317697481.

[7] Aaboud B, Bizet L, Saouab A, Nawab Y. Effect of the spatial variation of permeability on air bubble creation and compression. J Reinf Plast Compos 2020;39(7–8):285–98. http://dx.doi.org/10.1177/0731684419899475.

[8] Simacek P, Advani SG. A numerical model to predict fiber tow saturation during liquid composite molding. Compos Sci Technol 2003;63(12):1725–36. http://dx.doi.org/10.1016/S0266-3538(03)00155-6.

[9] Ruiz E, Achim V, Soukane S, Trochu F, Bréard J. Optimization of injection flow rate to minimize micro/macro-voids formation in resin transfer molded composites. Compos Sci Technol 2006;66(3):475–86. http://dx.doi.org/10.1016/j.compscitech.2005.06.013.

[10] Dunkers JP, Lenhart JL, Kueh SR, van Zanten JH, Advani SG, Parnas RS. Fiber optic flow and cure sensing for liquid composite molding. Opt Lasers Eng 2001;35(2):91–104. http://dx.doi.org/10.1016/S0143-8166(00)00110-X.

[11] PARNAS RS, PHELAN FR. The effect of heterogeneous porous media on mold filling in resin transfer molding. SAMPE Q 1991;22(2). 53–60UR–https://pascal--francis.inist.fr/vibad/index.php?action=getRecordDetail{&}idt=19539399.

[12] Sadiq T, Advani SG, PARNAS RS. Experimental investigation of transverse flow through aligned cylinders. Int J Multiph Flow 1995;21(5):755–74. http://dx.doi.org/10.1016/0301-9322(95)00026-T.

[13] Kuentzer N, Simacek P, Advani SG, Walsh S. Permeability characterization of dual scale fibrous porous media. Composites A 2006;37(11):2057–68. http://dx.doi.org/10.1016/j.compositesa.2005.12.005.

[14] Gebart BR. Permeability of unidirectional reinforcements for RTM. J Compos Mater 1992;26(8):1100–33. http://dx.doi.org/10.1177/002199839202600802.

[15] Bruschke MV, Advani SG. A numerical approach to model non-isothermal viscous flow through fibrous media with free surfaces. Internat J Numer Methods Fluids 1994;19(7):575–603. http://dx.doi.org/10.1002/fld.1650190704.

[16] Gommer F, Endruweit A, Long AC. Influence of the micro-structure on saturated transverse flow in fibre arrays. J Compos Mater 2018;52(18):2463–75. http://dx.doi.org/10.1177/0021998317747954.

[17] Yazdchi K, Srivastava S, Luding S. Microstructural effects on the permeability of periodic fibrous porous media. Int J Multiph Flow 2011;37(8):956–66. http://dx.doi.org/10.1016/j.ijmultiphaseflow.2011.05.003.

[18] Patel N, Rohatgi V, Lee LJ. Micro scale flow behavior and void formation mechanism during impregnation through a unidirectional stitched fiberglass mat. Polym Eng Sci 1995;35(10):837–51. http://dx.doi.org/10.1002/pen.760351006.

[19] Patel N, Lee LJ. Modeling of void formation and removal in liquid composite molding. Part I: Wettability analysis. Polym Compos 1996;17(1):96–103. http://dx.doi.org/10.1002/pc.10594.

[20] Patel N, Lee LJ. Modeling of void formation and removal in liquid composite molding. Part II: Model development and implementation. Polym Compos 1996;17(1):104–14. http://dx.doi.org/10.1002/pc.10595.

[21] Kamei Y, Ohgaki H, Ueno I. Impregnation process of viscous fluid in woven fibre bundles driven by pressure difference. In: FPCM 14, 2018. (30 May-1 June).

[22] Lystrup C, George A, Zobell B, Boster K, Childs C, Girod H, Fullwood D. Optical measurement of voids in situ during infusion of carbon reinforcements. J Compos Mater 2020;002199832095982. http://dx.doi.org/10.1177/0021998320959820.

[23] Mehdikhani M, Gorbatikh L, Verpoest I, Lomov SV. Voids in fiber-reinforced polymer composites: A review on their formation, characteristics, and effects on mechanical performance. J Compos Mater 2019;53(12):1579–669. http://dx.doi.org/10.1177/0021998318772152.

[24] Pillai KM, Advani SG. Numerical simulation of unsaturated flow in woven fiber preforms during the resin transfer molding process. Polym Compos 1998;19(1):71–80. http://dx.doi.org/10.1002/pc.10077.

[25] Staffan Lundström T, Frishfelds V, Jakovics A. Bubble formation and motion in non-crimp fabrics with perturbed bundle geometry. Composites A 2010;41(1):83–92. http://dx.doi.org/10.1016/j.compositesa.2009.05.012.

[26] DeValve C, Pitchumani R. Simulation of void formation in liquid composite molding processes. Composites A 2013;51:22–32. http://dx.doi.org/10.1016/j.compositesa.2013.03.016.

[27] Gascón L, García JA, LeBel F, Ruiz E, Trochu F. Numerical prediction of saturation in dual scale fibrous reinforcements during liquid composite molding. Composites A 2015;77:275–84. http://dx.doi.org/10.1016/j.compositesa.2015.05.019.

[28] Matsuzaki R, Seto D, Naito M, Todoroki A, Mizutani Y. Analytical prediction of void formation in geometrically anisotropic woven fabrics during resin transfer molding. Compos Sci Technol 2015;107:154–61. http://dx.doi.org/10.1016/j.compscitech.2014.12.013.

[29] Matsuzaki R, Naito M, Seto D, Todoroki A, Mizutani Y. Analytical prediction of void distribution and a minimum-void angle in anisotropic fabrics for radial injection resin transfer molding. Express Polym Lett 2016;10(10):860–72. http://dx.doi.org/10.3144/expresspolymlett.2016.80.

[30] Liu Y, Moulin N, Bruchon J, Liotier P-J, Drapier S. Towards void formation and permeability predictions in LCM processes: A computational bifluid–solid mechanics framework dealing with capillarity and wetting issues. C R Acad Sci, Paris 2016;344(4–5):236–50. http://dx.doi.org/10.1016/j.crme.2016.02.004.

[31] Patiño Arcila I, Power H, Nieto Londoño C, Flórez Escobar W. Boundary element method for the dynamic evolution of intra-tow voids in dual-scale fibrous reinforcements using a Stokes–Darcy formulation. Eng Anal Bound Elem 2018;87:133–52. http://dx.doi.org/10.1016/j.enganabound.2017.11.014.

[32] Moon Koo Kang, Woo Il Lee, Thomas Hahn H. Formation of microvoids during resin-transfer molding process. Compos Sci Technol 2000;60(12):2427–34. http://dx.doi.org/10.1016/S0266-3538(00)00036-1.

[33] Nedanov PB, Advani SG. Numerical computation of the fiber preform permeability tensor by the homogenization method. Polym Compos 2002;23(5):758–70. http://dx.doi.org/10.1002/pc.10474.

[34] Lawrence JM, Neacsu V, Advani SG. Modeling the impact of capillary pressure and air entrapment on fiber tow saturation during resin infusion in LCM. Composites A 2009;40(8):1053–64. http://dx.doi.org/10.1016/j.compositesa.2009.04.013.

[35] Gourichon B, Binetruy C, Krawczak P. A new numerical procedure to predict dynamic void content in liquid composite molding. Composites A 2006;37(11):1961–9. http://dx.doi.org/10.1016/j.compositesa.2005.12.017.

[36] Schell J, Deleglise M, Binetruy C, Krawczak P, Ermanni P. Numerical prediction and experimental characterisation of meso-scale-voids in liquid composite moulding. Composites A 2007;38(12):2460–70. http://dx.doi.org/10.1016/j.compositesa.2007.08.005.

[37] Lundström TS, Stenberg R, Bergström R, Partanen H, Birkeland PA. In-plane permeability measurements: A nordic round-robin study. Composites A 2000;31(1):29–43. http://dx.doi.org/10.1016/S1359-835X(99)00058-5.

[38] Vernet N, Ruiz E, Advani S, Alms JB, Aubert M, Barburski M, Barari B, Beraud JM, Berg DC, Correia N, Danzi M, Delavière T, Dickert M, Di Fratta C, Endruweit A, Ermanni P, Francucci G, Garcia JA, George A, Hahn C, Klunker F, Lomov SV, Long A, Louis B, Maldonado J, Meier R, Michaud V, Perrin H, Pillai K, Rodriguez E, Trochu F, Verheyden S, Wietgrefe M, Xiong W, Zaremba S, Ziegmann G. Experimental determination of the permeability of engineering textiles: Benchmark II. Composites A 2014;61:172–84. http://dx.doi.org/10.1016/j.compositesa.2014.02.010.

[39] Weitzenböck JR, Shenoi RA, Wilson PA. A unified approach to determine principal permeability of fibrous porous media. Polym Compos 2002;23(6):1132–50. http://dx.doi.org/10.1002/pc.10507.

[40] Arbter R, Beraud JM, Binetruy C, Bizet L, Bréard J, Comas-Cardona S, Demaria C, Endruweit A, Ermanni P, Gommer F, Hasanovic S, Henrat P, Klunker F, Laine B, Lavanchy S, Lomov SV, Long A, Michaud V, Morren G, Ruiz E, Sol H, Trochu F, Verleye B, Wietgrefe M, Wu W, Ziegmann G. Experimental determination of the permeability of textiles: A benchmark exercise. Composites A 2011;42(9):1157–68. http://dx.doi.org/10.1016/j.compositesa.2011.04.021.

[41] May D, Aktas A, Advani SG, Berg DC, Endruweit A, Fauster E, Lomov SV, Long A, Mitschang P, Abaimov S, Abliz D, Akhatov I, Ali MA, Allen TD, Bickerton S, Bodaghi M, Caglar B, Caglar H, Chiminelli A, Correia N, Cosson B, Danzi M, Dittmann J, Ermanni P, Francucci G, George A, Grishaev V, Hancioglu M, Kabachi MA, Kind K, Deléglise-Lagardère M, Laspalas M, Lebedev OV, Lizaranzu M, Liotier P-J, Middendorf P, Morán J, Park C-H, Pipes RB, Pucci MF, Raynal J, Rodriguez ES, Schledjewski R, Schubnel R, Sharp N, Sims G, Sozer EM, Sousa P, Thomas J, Umer R, Wijaya W, Willenbacher B, Yong A, Zaremba S, Ziegmann G. In-plane permeability characterization of engineering textiles based on radial flow experiments: A benchmark exercise. Composites A 2019;121:100–14. http://dx.doi.org/10.1016/j.compositesa.2019.03.006.

[42] LeBel F, Fanaei AE, Ruiz É, Trochu F. Prediction of optimal flow front velocity to minimize void formation in dual scale fibrous reinforcements. Int J Mater Form 2014;7(1):93–116. http://dx.doi.org/10.1007/s12289-012-1111-x.

[43] Pucci MF, Liotier P-J, Drapier S. Capillary wicking in a fibrous reinforcement – Orthotropic issues to determine the capillary pressure components. Composites A 2015;77:133–41. http://dx.doi.org/10.1016/j.compositesa.2015.05.031.

[44] Ahn KJ, Seferis JC, Berg JC. Simultaneous measurements of permeability and capillary pressure of thermosetting matrices in woven fabric reinforcements. Polym Compos 1991;12(3):146–52. http://dx.doi.org/10.1002/pc.750120303.